Hindawi
Geofluids
Volume 2021, Article ID 6631444, 17 pages
https://doi.org/10.1155/2021/6631444

Research Article

Research on the Evolution Characteristics of Floor Stress and Reasonable Layout of Roadways in Deep Coal Mining

Yang Yu[1,2] **Lianying Zhang**[1] **Jianfei Lu**[1] **Dingchao Chen**[1] **Xiangqian Zhao**[3] **and Limin Liu**[2]

[1]*School of Civil Engineering, Xuzhou University of Technology, Xuzhou 221111, China*
[2]*Tai'an Fangzhou Mining Technology Co., Ltd., Tai'an 271024, China*
[3]*School of Mining Engineering, China University of Mining and Technology, Xuzhou 221111, China*

Correspondence should be addressed to Lianying Zhang; zhanglianying@xzit.edu.cn and Jianfei Lu; 20180702121@xzit.edu.cn

Received 14 November 2020; Revised 4 December 2020; Accepted 4 March 2021; Published 15 March 2021

Academic Editor: Ondra Sracek

The safe and efficient mining of deep coal resources is severely restricted by the dynamic disasters caused by high gas and high ground stress. Taking a deep mine in China as the research background, a mechanical model of the front supporting stress with the working face was constructed through theoretical calculations. Based on the limit equilibrium theory, the stress distribution in the plastic zone and the elastic zone of the lateral working face was derived; based on semi-infinite plane mechanics model, the floor vertical and horizontal stress distribution was deduced. Then, the roadway surrounding rock stress and displacement field distribution evolution characteristics were revealed through numerical simulation. On this basis, the reasonable floor gas drainage roadway (FGDR) layout was determined: internal staggered layout was used with FGDR, the vertical distance to the working face is 20 m, and the horizontal distance to the working face end is 15 m; the open-off cut of FGDR was arranged in an external staggered layout, the vertical distance to the working face is 20 m, and the horizontal distance to the open-off cut of the working face is 15 m. It is an important practical significance for the layout of FGDR, the control of surrounding rocks, and the improvement of gas drainage effects under similar conditions through the research results.

1. Introduction

Among the main coal mining countries in the world, such as the United States, Australia, Germany, the United Kingdom, Poland, and Russia, other mining industries are relatively developed, while Germany and Russia enter deep mining earlier. There are 30 mines in Russia's Donbass mining area with mining depth of 1200-1350 m [1–6]. The average mining depth of a Polish coal mine is 690 m, and the deepest coal mine has reached 1300 m. The coal mining depth in Japan and Britain has reached 1125 m and 1100 m, respectively. China is rich in coal resources and widely distributed, and its coal output ranks first in the world. 76.3% of the total coal resources are buried more than 600 m, and 59.5% are buried more than 1000 m. With the increase of mining intensity, the mining depth of China's coal mines increases at a rate of 8-12 m per year. A large number of coal mines have entered the deep mining stage rapidly. There are 55 coal mines with mining depth of more than 1000 m, mainly distributed in Shandong, Henan, Anhui, Hebei, Heilongjiang, Jilin, and Liaoning in the eastern and northeast regions. The maximum mining depth reaches 1501 m [7–12]. The specific distribution is shown in Figure 1. It is estimated that in the next 10 years, most of the existing coal mines will enter the deep mining environment of 1000-1500 m. With the increase of coal mining depth, it is mainly faced with the problems of high gas, high ground stress, and high ground temperature, especially the compound dynamic disaster caused by high gas and high ground stress, which seriously restricts the safe production and becomes the bottleneck restricting the safe and efficient mining of deep coal resources.

The deep rock mass is in the harsh environment of "high ground stress, high temperature, and high karst

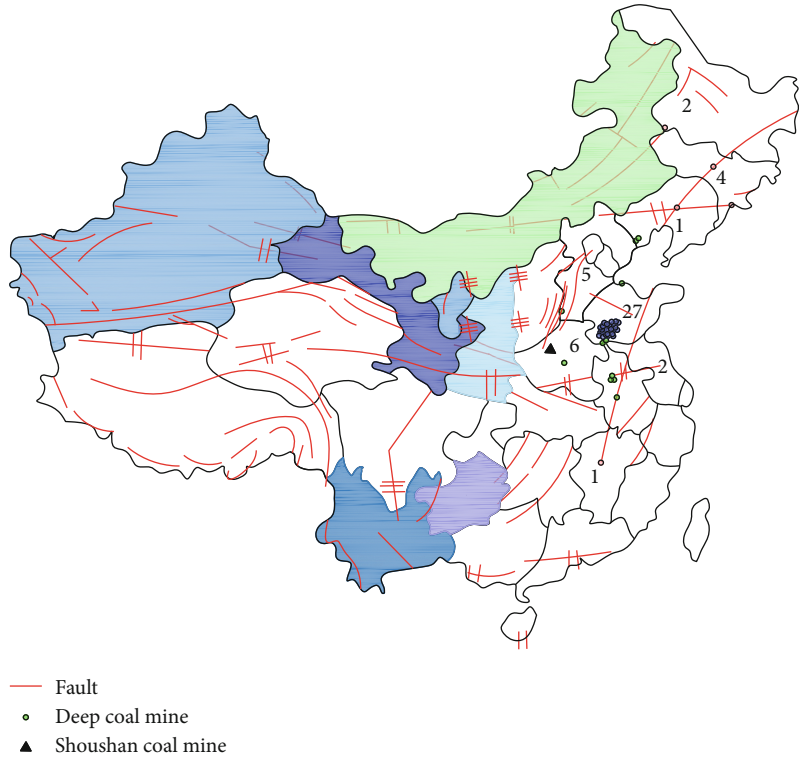

Figure 1: Distribution of coal mines with a depth of more than 1000 m in China.

water pressure and dynamic disturbance of blasting and mechanical excavation." The mine pressure of roadway is strong, and maintenance is difficult. According to incomplete statistics, when the depth of a mine is 1000 m, the repair rate of roadway is about 3-15 times that of 500-600 m under the same conditions, and the serious disrepair rate of some mine roadways is more than 20% [13, 14]. Shoushan No. 1 Coal Mine of Henan Pingbao Coal Industry Co., Ltd. has an average buried depth of more than 750 m, stratum dip angle of 8-12°, and well-developed geological structure. It is a high gas outburst mine. Under the condition that there is no mining protective layer to realize regional outburst prevention, only through the construction of FGDR, cross layer drilling was used to implement predrainage outburst prevention technology for coal seam gas. Due to the double effects of driving and mining stress, the surrounding rock of roadway, especially the floor, is continuously deformed. The key parameters such as vertical distance and horizontal distance between FGDR and coal seam roadway directly affect the amount of drilling work, gas drainage amount, and protection effect. Therefore, reasonable roadway layout can not only eliminate the gas disaster caused by roadway excavation and working face mining but also effectively reduce the influence of roadway excavation and working face mining on floor gas roadway, making the roadway in low stress environment for a long time and greatly reducing the maintenance difficulty. Therefore, the location selection of FGDR has important practical significance for its own stability and gas control effect.

The evolution characteristics of floor stress distribution caused by upper coal seam mining have great influence on the location selection and surrounding rock control of FGDR. At present, the research results of the distribution and evolution characteristics of the floor rock layer in the upper coal seam working face are mainly based on the finite element numerical calculation and similar material simulation experiments and lack of theoretical research on the floor rock mass movement. At the same time, the floor stress field monitoring research has the characteristics of difficult testing and high cost, and the research progress is slow [15–20]. In addition, a large number of domestic and foreign scholars have made a lot of research results on the influence of floor level and gas layer [21–26]. However, in view of the differences of mine hydrogeological conditions and mining technology level, the existing research results still do not have universal applicability. Therefore, for the high gas outburst mine under specific conditions, the selection of reasonable FGDR layout still needs to be combined with the field production conditions for differential research.

2. The Project Overview

Shoushan No. 1 mine is located in Pingdingshan City, Henan Province, China. The designed annual production capacity of the mine is 0.3 Mt, and the service life is 92 years. At present, No. 15 and No. 16 coal seams are mainly mined, and the coal seam structure is relatively simple. The direct roof of the coal seam is mainly composed of sandy mudstone and mudstone, occasionally with fine-grained sandstone and siltstone. The

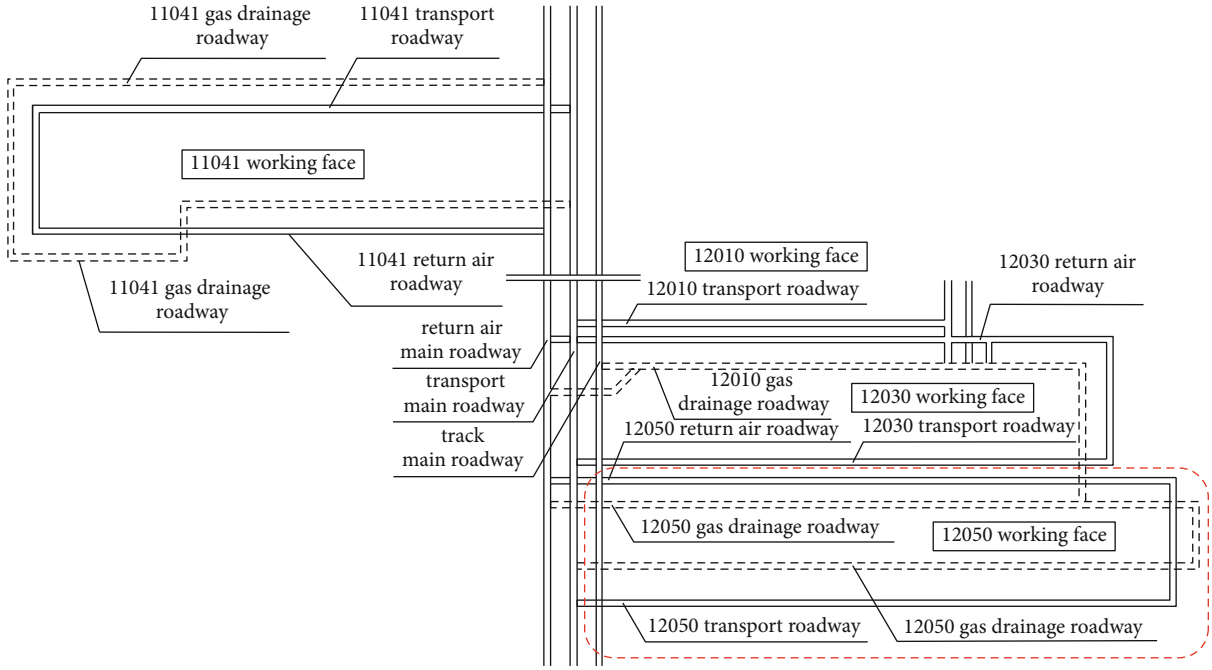

Figure 2: The excavation engineering plan.

Table 1: The physical and mechanical properties of roadway surrounding rock.

Lithology	Bulk density (kN·m^3)	Thickness (m)	Compressive strength (MPa)	Elastic modulus (GPa)	Poisson ratio	Interfriction angle (°)	Cohesion (MPa)	Tensile strength (MPa)
Fine sandstone	27.5	32	25.7	10.0	0.20	40	6.0	6.0
Sandy mudstone	25.3	8.0	9.4	3.5	0.22	34	2.5	2.5
No. 15 coal seam	13.6	3.5	4.2	2.5	0.25	19	1.5	1.5
Mudstone	24.5	3.5	7.2	2.5	0.23	32	2.0	2.0
No. 16 coal seam	13.6	6.5	4.7	2.0	0.23	32	1.5	1.4
Fine sandstone	27.5	5.0	25.7	10.0	0.20	40	6.0	6.0
Sandy mudstone	25.3	12	9.4	4.5	0.22	34	5.0	3.2
Limestone	28.0	13	30	10.0	0.20	40	8.0	7.2

floor is mainly composed of mudstone, and part of it is fine-grained sandstone, with occasional false bottom of carbonaceous mudstone. The hydrogeological conditions of the mine are simple, the main coal seam has outburst risk, the gas content is 10.46 m^3/t, the gas pressure is 1.38 MPa, there is spontaneous combustion tendency, the spontaneous combustion period is 4-6 months, and there is coal dust explosion risk. Based on the safety mining of 12050 working face as the engineering background, the evolution characteristics of floor stress distribution caused by 12050 working face mining were revealed in the paper. On this basis, the layout layer of FGDR is selected, and the relative spatial position relationship between FGDR and upper working face is determined, which creates favorable conditions for gas drainage in 12050 working face. The plan of excavation engineering is shown in Figure 2, and the physical and mechanical properties of rock stratum are shown in Table 1.

3. Study on Evolution Characteristics of Stress Distribution in Coal Seam Floor

The research on the evolution characteristics of floor stress distribution caused by coal mining is of great practical significance to master the deformation law and failure characteristics of floor rock, to predict water inrush from floor, and to design the position and maintenance technology of floor roadway. The distribution of lateral support stress caused by working face mining is determined by means of theoretical calculation and numerical simulation, and the distribution law of floor rock stress after coal mining is discussed.

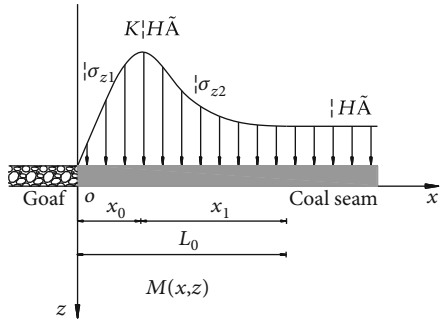

Figure 3: Mechanical model of support stress distribution in front of working face.

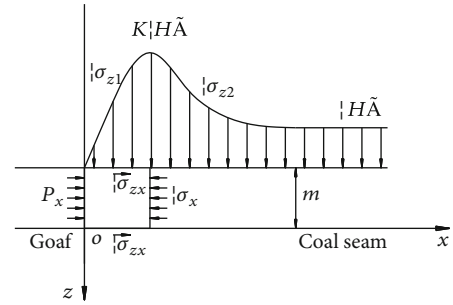

Figure 4: Mechanical model of limit equilibrium in coal pillar.

3.1. Theoretical Calculation Research. After coal mining, the evolution characteristics of floor stress distribution depend on the propagation law of lateral support stress in floor, as shown in Figure 3. Among them, x_0 is the range of plastic zone in front of working face; σ_{z1} is the inner supporting stress of plastic zone; x_1 is the scope of elastic zone; σ_{z2} is the inner supporting stress of elastic zone; l_0 is the total width of elastic zone and plastic zone; $K\gamma h$ is the peak value of vertical stress, which is located at the interface of elastic-plastic zone; K is the stress concentration factor; γh is the original rock stress of coal seam floor.

When the coal strength is less than the roof strength, the following assumptions are made: (1) the coal is a continuous, homogeneous, and isotropic elastic body; (2) the displacement and deformation of the coal pillar before yielding are small; (3) the shear failure of the coal pillar occurs, and the shear failure surface is parallel to the coal seam; (4) when the coal pillar yields locally, the yield area is regarded as the elastic limit state, and the coal body in the yield area is regarded as a linear elastic body; (5) there is no weak plane in coal pillar. Due to the accumulation of coal gangue at the bottom of goaf and the subsidence of coal pillar under the action of self-weight stress of overlying strata, the lower part of coal pillar can be regarded as in three-dimensional stress state, and its stability is strengthened. Therefore, the stress state of the upper and middle coal pillar is mainly considered in the study.

Because the strength of the strata is greater than that of the coal, the transverse deformation of the coal seam is greater than that of the rock under the self-weight stress of the overlying strata. Therefore, the coal seam has a trend of outward movement relative to the rock stratum, that is, the friction force formed between the coal seam and the roof, that is, the shear stress, as shown in Figure 4. τ_{xz} is the shear stress, σ_x is the horizontal stress in the coal pillar, P_x is the support strength of the side entry in the goaf, and m is the thickness of the coal seam.

Under the action of self-weight stress of overlying strata, the coal body will have shear failure under the action of compressive stress, and the failure mode conforms to Mohr-Coulomb criterion. Taking a cross section of coal pillar as the research object, its stress is about the neutral plane symmetry, and the stress of coal pillar can be regarded as plane strain problem. Therefore, the differential equation of the plane strain problem is satisfied.

$$\left.\begin{aligned} &\frac{\partial \sigma_x}{\partial x} + \frac{\partial \tau_{xz}}{\partial z} = 0, \\ &\frac{\partial \tau_{xz}}{\partial x} + \frac{\partial \sigma_z}{\partial z} = 0, \\ &\tau_{xz} = -(\sigma_z \tan \varphi + C). \end{aligned}\right\} \tag{1}$$

The lateral support stress σ_{z1} and shear stress τ_{xz} in the limit equilibrium zone x_0 are as follows:

$$\left.\begin{aligned} \sigma_{z1} &= \left(\frac{C}{\tan \varphi} + \frac{P_x}{A}\right) e^{(2 \tan \varphi / mA)x} - \frac{C}{\tan \varphi}, \\ \tau_{xy} &= -\left(C + \frac{P_x \tan \varphi}{A}\right) e^{(2 \tan \varphi / mA)x}. \end{aligned}\right\} \tag{2}$$

According to the equilibrium relation, there is $\sum F_X = 0$, that is,

$$m(\sigma_x{}^e + d\sigma_x{}^e) - m\sigma_x{}^e + 2f\sigma_z{}^e dx = 0. \tag{3}$$

In addition, $\sigma_x{}^e = A\sigma_z{}^e$ is substituted into equation (3) to obtain the stress distribution in elastic zone:

$$\sigma_{z2} = K\gamma H e^{(2f/mA)(x_0 - x)}. \tag{4}$$

When $x = x_0 + x_1, \sigma_y = \gamma H$, the elastic zone width is obtained by substituting equation (4):

$$x_1 = \frac{mA}{2f} \ln K. \tag{5}$$

As shown in Figure 5, take any point $M(x, z)$ on the bottom plate, take any micro segment $d\xi$ along the x direction, and regard the force $dP = Qd\xi$ as a tiny concentrated force.

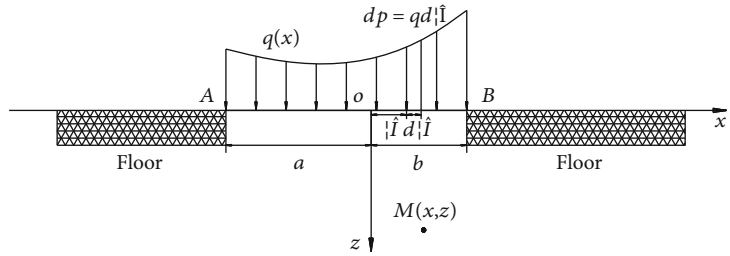

Figure 5: Model of distributed load acting on semi-infinite plane boundary.

The stress state formed by the tiny concentrated force at point M is as follows:

$$\left.\begin{aligned} d\sigma_z &= -\frac{2qd\xi}{\pi}\frac{z^3}{\left[(x-\xi)^2+z^2\right]^2},\\ d\sigma_x &= -\frac{2qd\xi}{\pi}\frac{z(x-\xi)^2}{\left[(x-\xi)^2+z^2\right]^2}. \end{aligned}\right\} \tag{6}$$

In order to obtain the effect of all distributed loads on point M, the stresses caused by each tiny concentrated force should be superimposed, that is to say, the integral of formula (1) from $\xi = -a$ to $\xi = b$ is obtained:

$$\left.\begin{aligned} \sigma_z &= -\frac{2}{\pi}\int_{-a}^{b}\frac{qz^3d\xi}{\left[(x-\xi)^2+z^2\right]^2},\\ \sigma_x &= -\frac{2}{\pi}\int_{-a}^{b}\frac{qz(x-\xi)^2d\xi}{\left[(x-\xi)^2+z^2\right]^2}. \end{aligned}\right\} \tag{7}$$

The vertical stress σ_{z11} and horizontal stress σ_{x11} produced by the load in the limit equilibrium zone are as follows:

$$\left.\begin{aligned} {\sigma_{z2}}^1 &= -\frac{2}{\pi}\int_{x_0}^{x_0+x_1}\frac{K\gamma He^{(2f/mA)(x_0-x)}z^3d\xi}{\left[(x-\xi)^2+z^2\right]^2},\\ {\sigma_{x2}}^1 &= -\frac{2}{\pi}\int_{x_0}^{x_0+x_1}\frac{K\gamma He^{(2f/mA)(x_0-x)}z(x-\xi)^2d\xi}{\left[(x-\xi)^2+z^2\right]^2}. \end{aligned}\right\} \tag{8}$$

Through the superposition of stresses, the stress of the bottom plate is obtained:

$$\left.\begin{aligned} \sigma_x &= {\sigma_{x1}}^1 + {\sigma_{x2}}^1,\\ \sigma_z &= {\sigma_{z1}}^1 + {\sigma_{z2}}^1. \end{aligned}\right\} \tag{9}$$

Among them are the following:

$$\left.\begin{aligned} {\sigma_{z1}}^1 &= -\frac{((C/\tan\varphi)+(P_x/A))e^{(2\tan\varphi/mA)x}-(C/\tan\varphi)}{\pi}\left[a\tan\left(\frac{x_0-x}{z}\right)+\frac{(x_0-x)z}{(x_0-x)^2+z^2}+a\tan\left(\frac{x}{z}\right)+\frac{xz}{x^2+z^2}\right],\\ {\sigma_{z2}}^1 &= -\frac{K\gamma He^{(2f/mA)(x_0-x)}}{\pi}\left[a\tan\left(\frac{x_0+x_1-x}{z}\right)+\frac{(x_0+x_1-x)z}{(x_0+x_1-x)^2+z^2}-a\tan\left(\frac{x_0-x}{z}\right)-\frac{(x_0-x)z}{(x_0-x)^2+z^2}\right],\\ {\sigma_{x1}}^1 &= -\frac{((C/\tan\varphi)+(P_x/A))e^{(2\tan\varphi/mA)x}-(C/\tan\varphi)}{\pi}\left[a\tan\left(\frac{x_0-x}{z}\right)-\frac{(x_0-x)z}{(x_0-x)^2+z^2}+a\tan\left(\frac{x}{z}\right)-\frac{xz}{x^2+z^2}\right],\\ {\sigma_{x2}}^1 &= -\frac{K\gamma He^{(2f/mA)(x_0-x)}}{\pi}\left[a\tan\left(\frac{x_0+x_1-x}{z}\right)-\frac{(x_0+x_1-x)z}{(x_0+x_1-x)^2+z^2}-a\tan\left(\frac{x_0-x}{z}\right)+\frac{(x_0-x)z}{(x_0-x)^2+z^2}\right]. \end{aligned}\right\} \tag{10}$$

Coal seam thickness $m = 3.5$ m; internal friction angle $\varphi = 25°$; cohesion $\sigma = 1.5$ MPa; horizontal lateral pressure coefficient $A = 1.3$; upper working face roadway support resistance $P_x = 0.3$ MPa; lateral support stress concentration coefficient $k = 3$; overburden rock average bulk density $\gamma = 25$ kN/m^2; working face buried depth $h = 750$ m; and friction coefficient between coal seam and roof and floor $f = 0.2$. By substituting equation (8), the stress state at any point of working face floor can be obtained. The distribution of internal stress in the range of 20 m behind the working face to 20 m in front of the working face and 30 m in the bottom plate is shown in Figure 6.

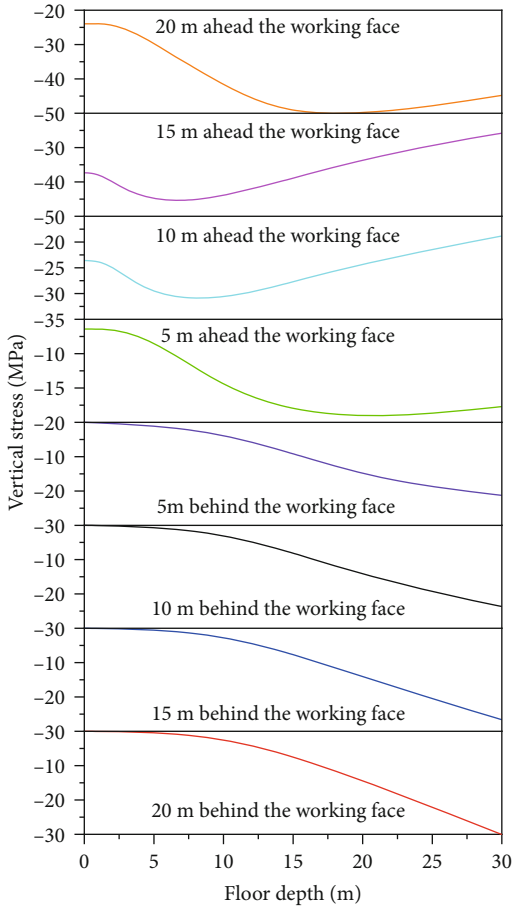

Figure 6: Stress distribution of floor.

It can be seen from Figure 6 that the stress distribution law of coal seam floor caused by working face mining is as follows:

(1) In the range of 5 m in front of the working face, the bearing capacity of coal body is sharply reduced and the vertical stress is low; the range of 10-20 m in front of the working face is the stress concentration area; along the depth direction of the coal seam floor, the vertical stress increases first and then decreases; in the range of 20 m behind the working face, the surrounding rock is in the area of vertical stress reduction when the depth of coal seam floor is less than 20 m

(2) In the range of 10-20 m in front of the working face, the vertical stress in the coal seam floor reaches the peak at the depth of 7 m and then decreases continuously; when the depth of coal seam floor is greater than 20 m, the vertical stress concentration coefficient is between 1.6 and 2.3, and the bearing capacity of surrounding rock is relatively high

3.2. Numerical Simulation Research. FLAC3D software is used to establish the model for numerical simulation. The stress distribution law of the floor after the transport roadway excavation and 12050 working face mining is mainly studied. The model size is length × width × height = 180 m × 80 m × 83.5 m, the total number of units is 321600, and the total number of nodes is 337348. The lateral displacement of the model is limited by the lateral displacement, and the vertical displacement is limited by the bottom surface. The upper surface is a stress boundary. A load of 15 MPa is applied to simulate the gravity stress of overlying rock mass. The material conforms to the Mohr-Coulomb model.

After the excavation of transport roadway in 12050 working face, the floor stress distribution law is shown in Figure 7. It can be seen from Figure 7 that (1) after roadway excavation, a large range of vertical stress reduction area is formed at the top and floor, the depth of the floor stress reduction area is 25 m, and the vertical stress is less than 10 MPa within the range of 7 m of the floor; (2) with the distance from the roadway floor, the stress gradient becomes more gentle; in the horizontal direction, the vertical stress of the floor first decreases and then increases, and the range of the plane stress reduction area with the floor depth of 14 m is the largest; (3) due to the influence of the soft floor and the close coal seam, a large range of horizontal stress concentration area is formed in the floor, with the floor depth greater than 10 m and the front and rear of the roadway 10 m.

After 12050 working face is mined, the vertical stress distribution law of the floor is shown in Figure 8. It can be seen from Figure 8 that (1) after deep mining, the ground pressure appears violently; within 20 m depth of the floor behind the working face, the stress decreases in a triangular distribution; the maximum stress in the area is only 3 MPa, and the stress concentration coefficient is greater than 2 within the range of 5-14 m in front of the working face; (2) when the depth of the floor exceeds 20 m, the depth of the floor is 15 m in front of the working face to 30 m behind the working face; within above range, the maximum vertical stress is 25 MPa, the minimum is 3 MPa, and the stress concentration coefficient is 0.15-1.25, which is the reasonable layout area of FGDR. In front of the working face, the stress concentration coefficient is more than 1.25, the surrounding rock stress of the roadway is large, and the maintenance is difficult; in the rear of the working face, considering that the length of the gas drilling hole should not be too long, the FGDR should not exceed 15 m behind the working face.

Therefore, considering the distribution law of floor stress field after transport roadway excavation and 12050 working face mining, the most suitable area for FGDR layout is floor depth greater than 20 m, 10-15 m in front of the working face and 10-15 m behind the working face.

4. Research on Layout of Gas Drainage Roadway in Coal Seam Floor

Considering the factors such as the length of gas drainage borehole which should not be too long, the effect of gas drainage, and the maintenance difficulty of FGDR, two kinds of FGDR layout are proposed: external staggered layout and internal staggered layout. The horizontal distance between FGDR and transport roadway of 12050 working face is

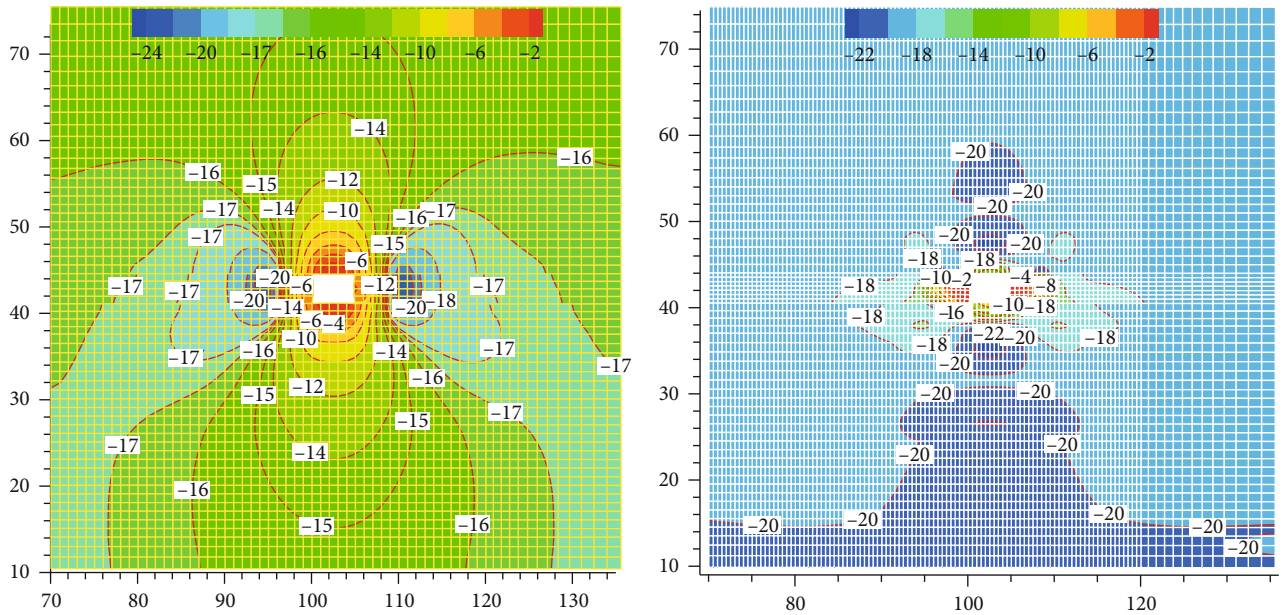

(a) Vertical stress

(b) Horizontal stress

Figure 7: Distribution law of floor stress field after roadway excavation.

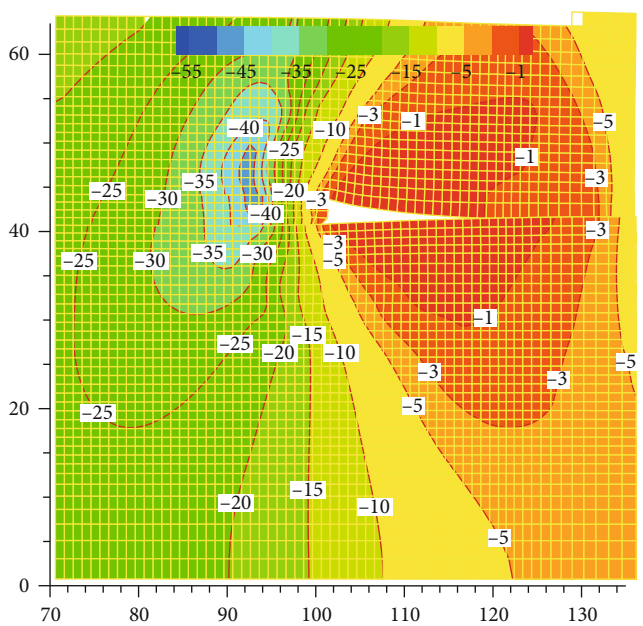

Figure 8: Distribution law of floor stress field after mining.

15 m, and vertical distance is 20 m, but the relative direction is different.

4.1. External Staggered Layout of FGDR. The numerical simulation model of external staggered layout of FGDR is established, as shown in Figure 9. In the figure, 12050 working face is excavated to half-length position, FGDR is arranged in sand and mudstone with floor thickness of 12 m, and left roadway is FGDR. The results show that the FGDR should be affected by three times of stress disturbance: (1) FGDR excavation, (2) 12050 working face transport roadway excavation, and (3) 12050 working face mining.

4.1.1. FGDR Excavation. After the excavation of FGDR, the distribution law of surrounding rock stress field is shown in Figure 10. The following can be seen from Figure 10:

(1) The maximum vertical stress is 25 MPa and the stress concentration factor is 1.5. In the range of 1-6 m depth of two sides, the vertical stress is greater than 18 MPa from the floor height of -1-4 m, which is elliptical distribution in the horizontal direction, while in shallow mining, the stress concentration coefficient is generally 1.1-1.2 under the same conditions

(2) The vertical stress forms a stress reduction zone in the top and bottom plates, ranging from 0 to 6 m in depth. From the left side width of -1-6 m, the range of stress reduction area is large, and the vertical stress is only 4 MPa in the range of 0-2 m depth of roof and floor. The shallow surrounding rock is in a low stress environment, which is conducive to roadway maintenance

(3) The horizontal stress forms a stress concentration area in the roof and floor of the roadway, and the range is 2-8 m depth of the roof and floor. The stress reduction area is formed on both sides of roadway, and the stress reduction area is 0-8 m depth of two sides and -2-5 m depth of floor

In addition, after the excavation of FGDR, the roof subsidence is 63.3 mm, the floor heave is 52.4 mm, and the two sides are moved closer by 80 mm.

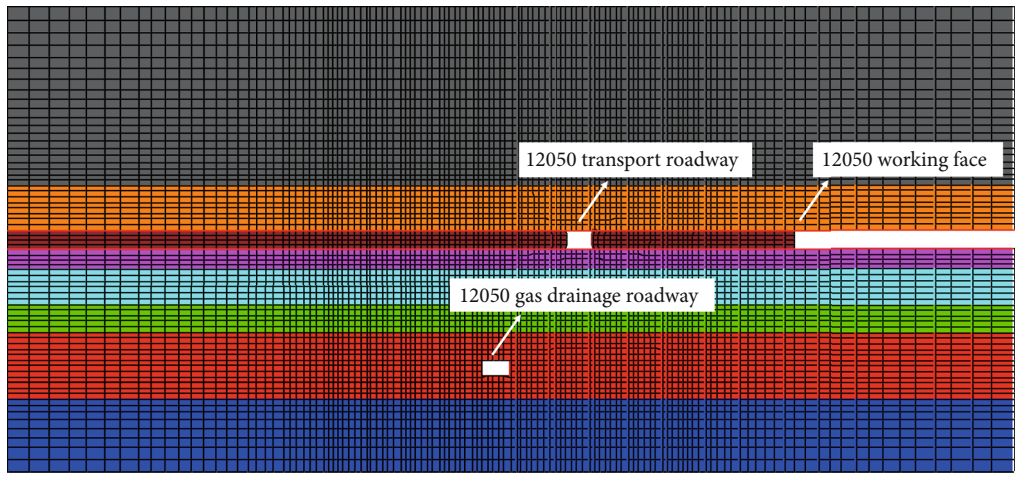

Figure 9: Numerical simulation model of staggered arrangement.

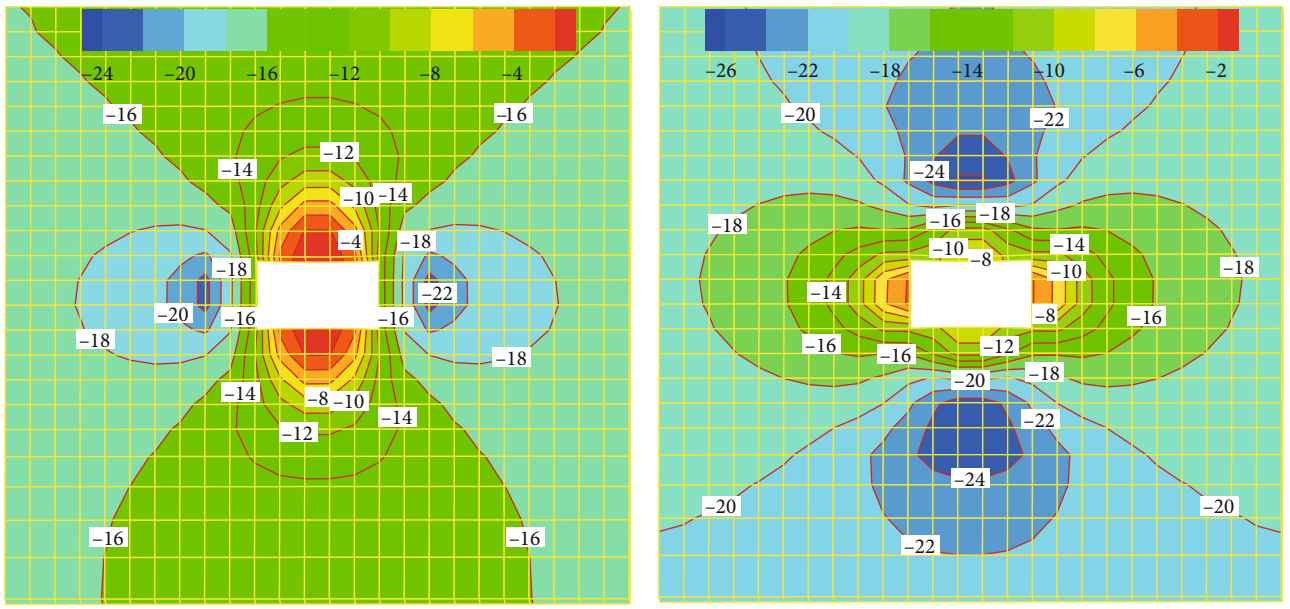

(a) Vertical stress

(b) Horizontal stress

Figure 10: Stress field distribution law of surrounding rock in gas drainage roadway with floor.

4.1.2. 12050 Working Face Transport Roadway Excavation. After the excavation of transport roadway in 12050 working face, the stress field distribution law of roadway surrounding rock is shown in Figures 11 and 12.

(1) The excavation of transport roadway is equivalent to the roof pressure relief of FGDR, and the surrounding rock stress is obviously transferred to the direction of transport roadway. The vertical stress of surrounding rock is 16 MPa at the right side depth of 9 m and 18 MPa at the left side depth of 8 m

(2) The horizontal stress and the vertical stress of the left side and the two sides of the FGDR increase slightly after the excavation of the transport roadway, while the vertical stress of the right side decreases. With the approach of the transport roadway, the stress difference before and after excavation gradually increases, with the maximum difference of 1.7 MPa. The FGDR is in a stress environment that is easy to be maintained

(3) After the excavation of the roadway, the vertical stress of the roof decreases and the vertical stress of the floor increases; the horizontal stress of the floor is basically unchanged, but the horizontal stress of the roof changes relatively large, and the stress decreases with the depth of the roof

In addition, after the excavation of the transport roadway, the roof subsidence is 62.2 mm, the floor heave is 55 mm, the left side is 49.4 mm, and the right side is 40.8 mm. To sum

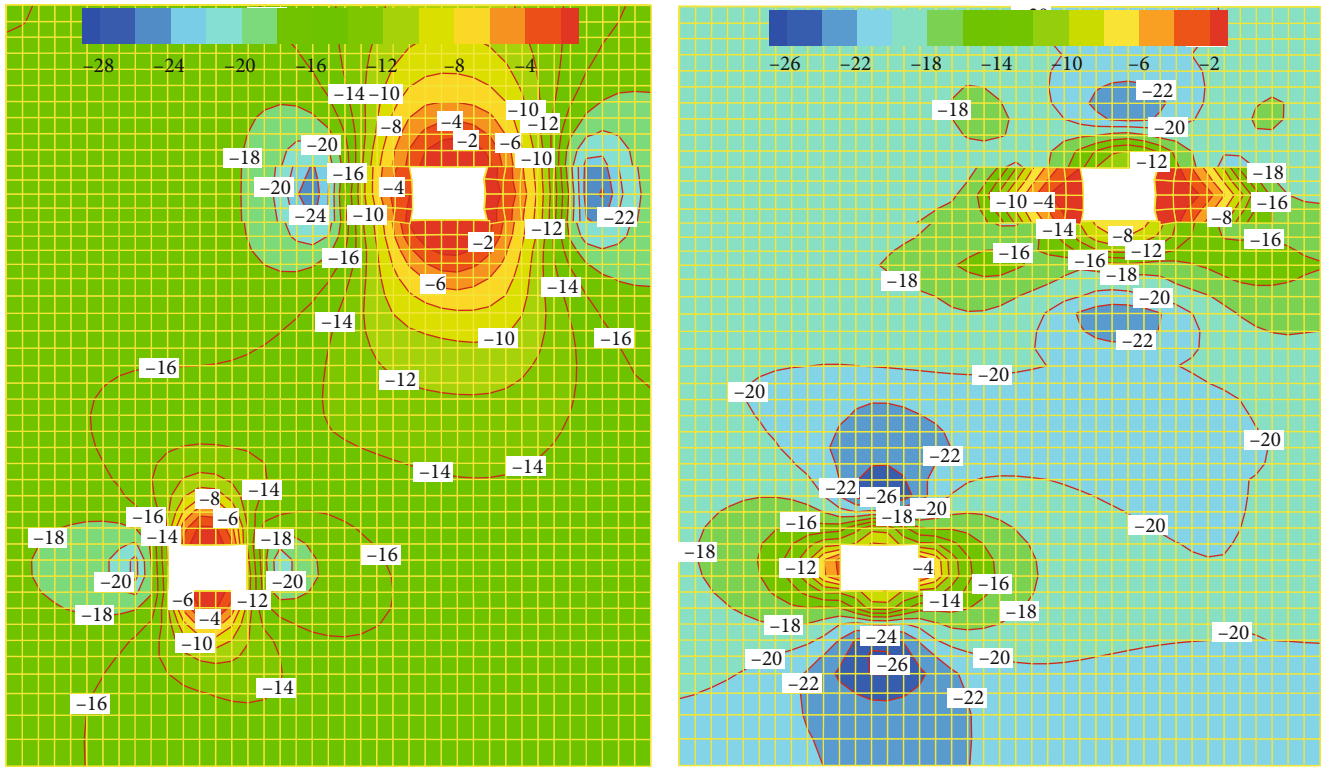

(a) Vertical stress (b) Horizontal stress

Figure 11: Distribution law of stress field in surrounding rock of roadway after excavation.

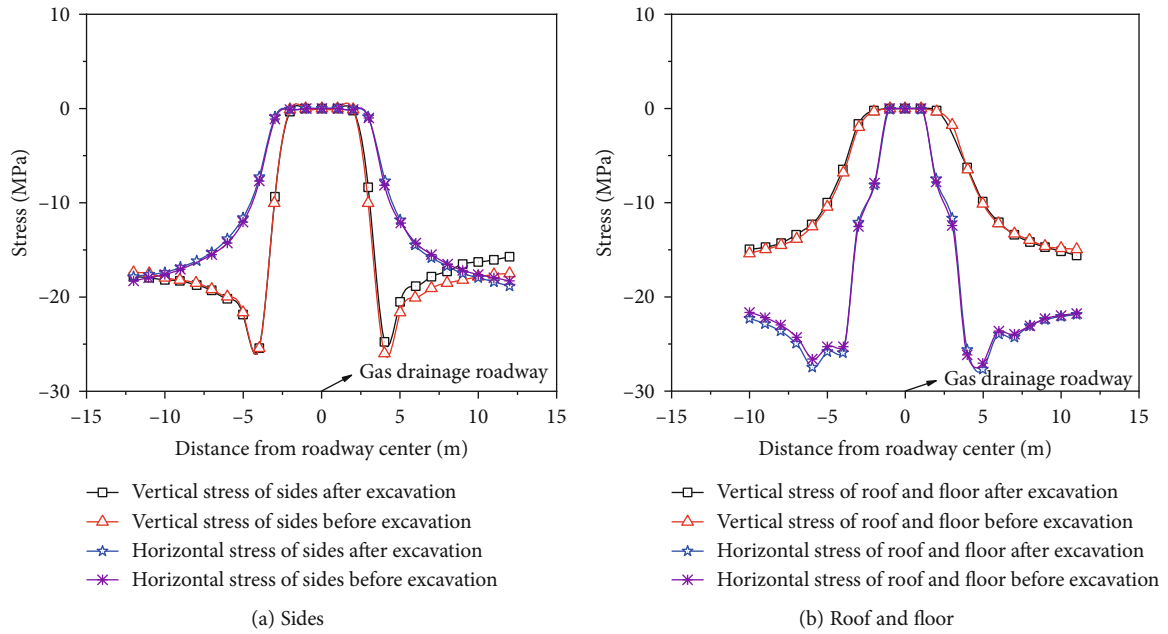

(a) Sides (b) Roof and floor

Figure 12: Stress distribution curve of roadway surrounding rock after excavation.

up, the influence of roadway excavation on the horizontal stress of surrounding rock is small, and the vertical stress distribution is relatively large, especially on the right side.

4.1.3. 12050 Working Face Mining. After mining in 12050 working face, the stress distribution law of surrounding rock of FGDR is shown in Figures 13 and 14.

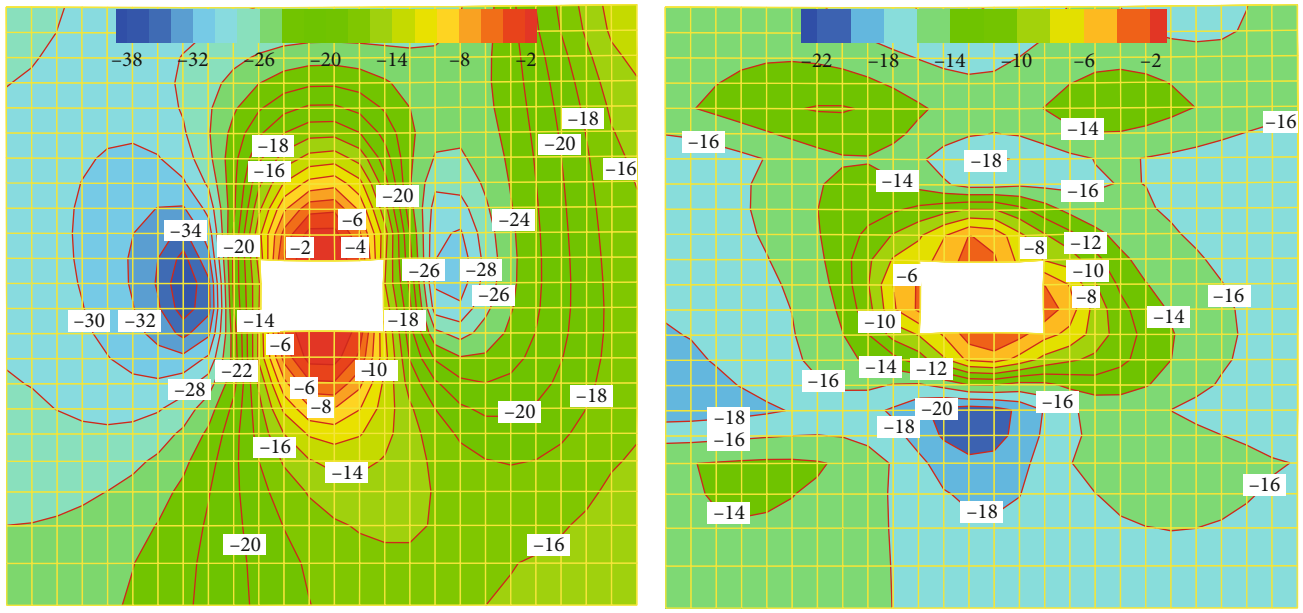

(a) Vertical stress (b) Horizontal stress

Figure 13: Distribution law of stress field in surrounding rock of roadway after mining.

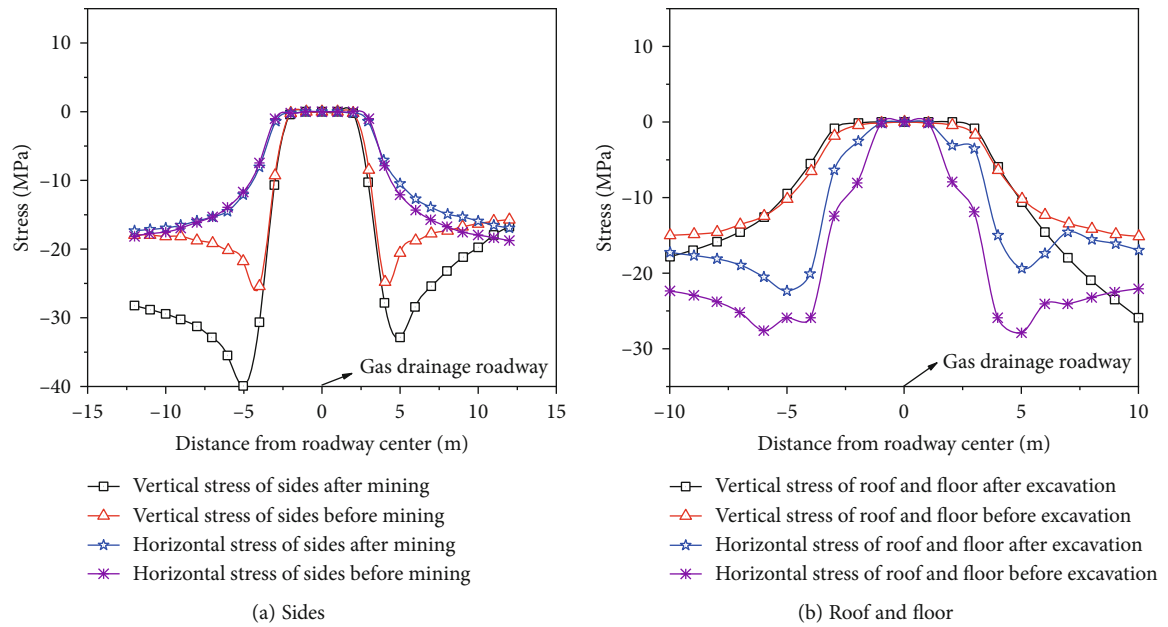

(a) Sides (b) Roof and floor

Figure 14: Stress distribution curve of roadway surrounding rock after mining.

(1) After mining in 12050 working face, the vertical stress of two sides of FGDR increased greatly, the peak value of vertical stress of left side reached 40.2 MPa, increased by 58.3%, and that of right side reached 33 MPa, with an increase of 33.1%; the peak position of vertical stress of two sides was transferred from 2 m to 3 m away from the roadway surface; the horizontal stress of left side remained basically unchanged, and the horizontal stress of right side decreased slightly

(2) After mining in 12050 working face, the horizontal stress of FGDR roof and floor presents irregular distribution, which is greatly affected by mining. The maximum reduction value of horizontal stress of roof and floor is 7.1 MPa, which is located at the depth of 5 m, with a decrease rate of 34.8%. The maximum reduction value of horizontal stress of floor is 10.9 MPa, which is located at the depth of 3 m, with a decrease rate of 72.7%. Judging from the horizontal stress distribution, the mining face has the greatest

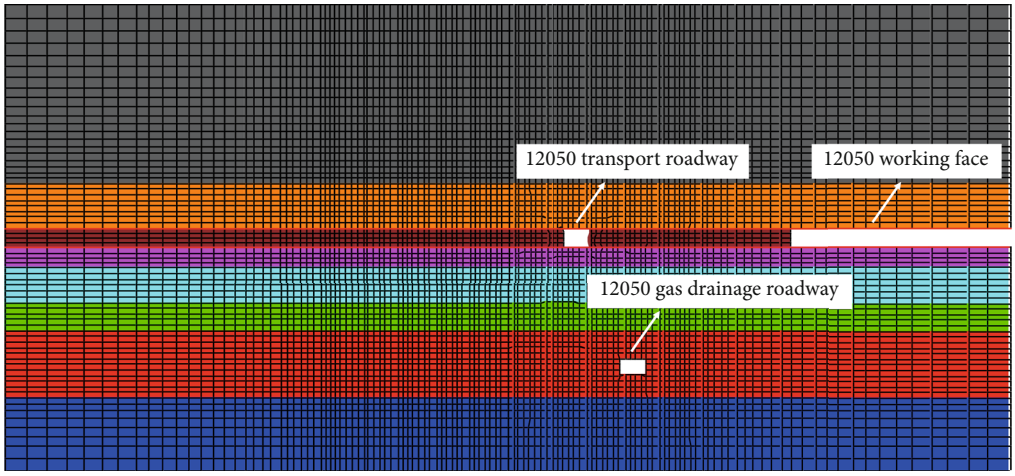

Figure 15: Numerical calculation model of internal staggered arrangement.

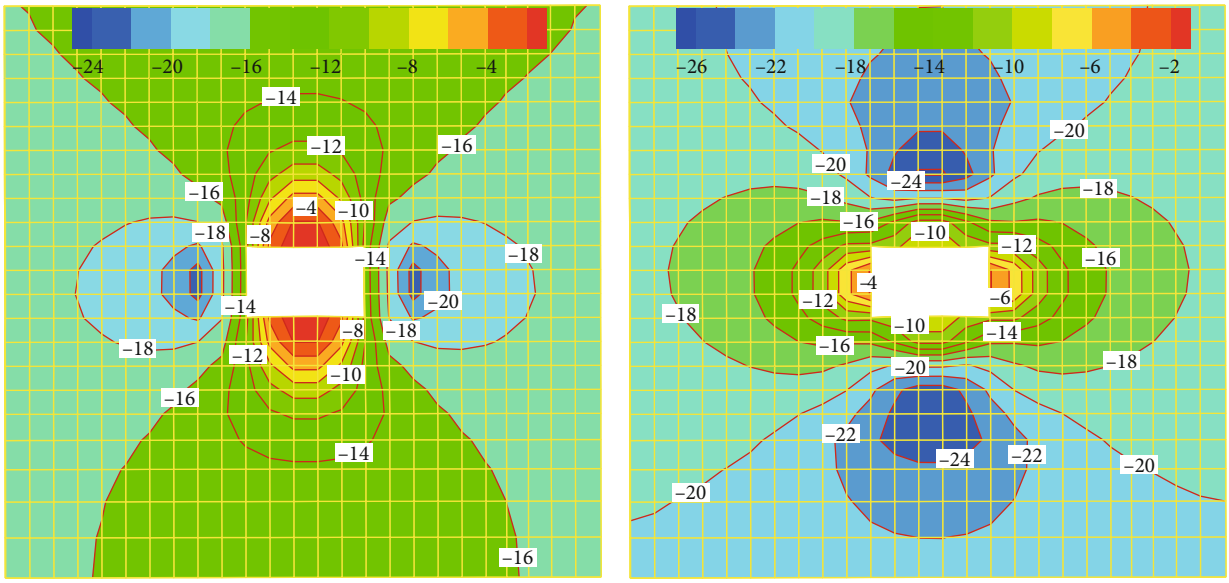

(a) Vertical stress

(b) Horizontal stress

Figure 16: Stress field distribution law of surrounding rock in gas drainage roadway with floor.

influence on the floor, followed by the roof, and the two sides have less influence

(3) After mining in 12050 working face, the vertical stress of the roof and floor of FGDR has increased, especially the vertical stress of the floor increases greatly, the maximum increase value is 12.2 MPa, the depth of the floor is 10 m, the increase rate is 78.2%, the maximum increase value of the second roof vertical stress is 2.6 MPa, located at the roof depth of 10 m, and the increase rate is 17.2%. Judging from the distribution of horizontal stress, the mining face has the greatest influence on the floor, followed by the left side, the right side next, and the roof the least

To sum up, when the FGDR is staggered outside, the stress concentration degree of the two sides and the floor is greatly increased, and the roof is also increased; the horizontal stress of the two sides is basically unchanged, while the horizontal stress of the roof and floor is greatly increased. In addition, after mining, the maximum roof subsidence is 150.3 mm, the floor heave is 47.8 mm, the left side is 104.3 mm, and the right side is 19.1 mm.

4.2. Internal Staggered Layout of FGDR. The numerical simulation model of internal staggered layout of FGDR is established, as shown in Figure 15. When the working face is excavated to half length, the FGDR is arranged in the sand and mudstone with the floor thickness of 12 m, and the middle roadway is the FGDR. The same as the external staggered layout, the FGDR will also be affected by three times of stress disturbance.

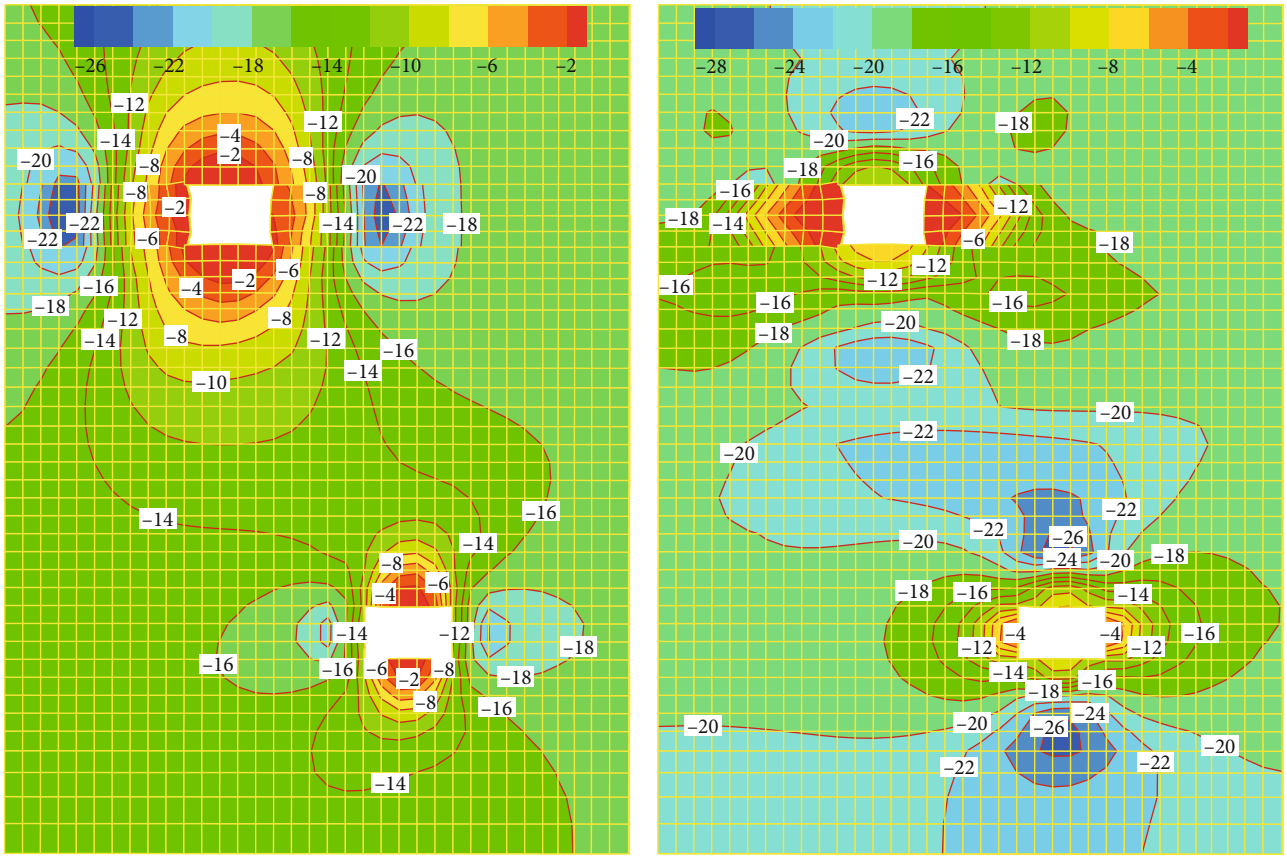

(a) Vertical stress (b) Horizontal stress

Figure 17: Distribution law of stress field in surrounding rock of roadway after excavation.

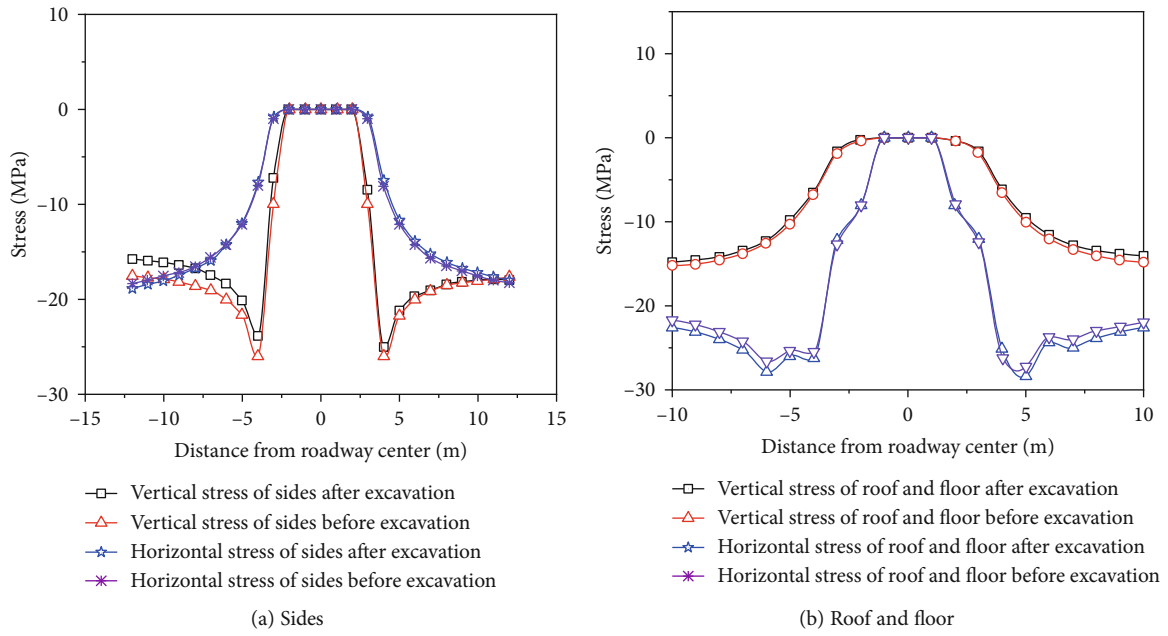

(a) Sides (b) Roof and floor

Figure 18: Stress distribution curve of roadway surrounding rock after excavation.

4.2.1. FGDR Excavation. After the excavation of FGDR, the distribution law of surrounding rock stress field is shown in Figure 16. Compared with the external staggered layout, the stress and displacement distribution characteristics of the surrounding rock of the FGDR have no significant difference, so we will not repeat it.

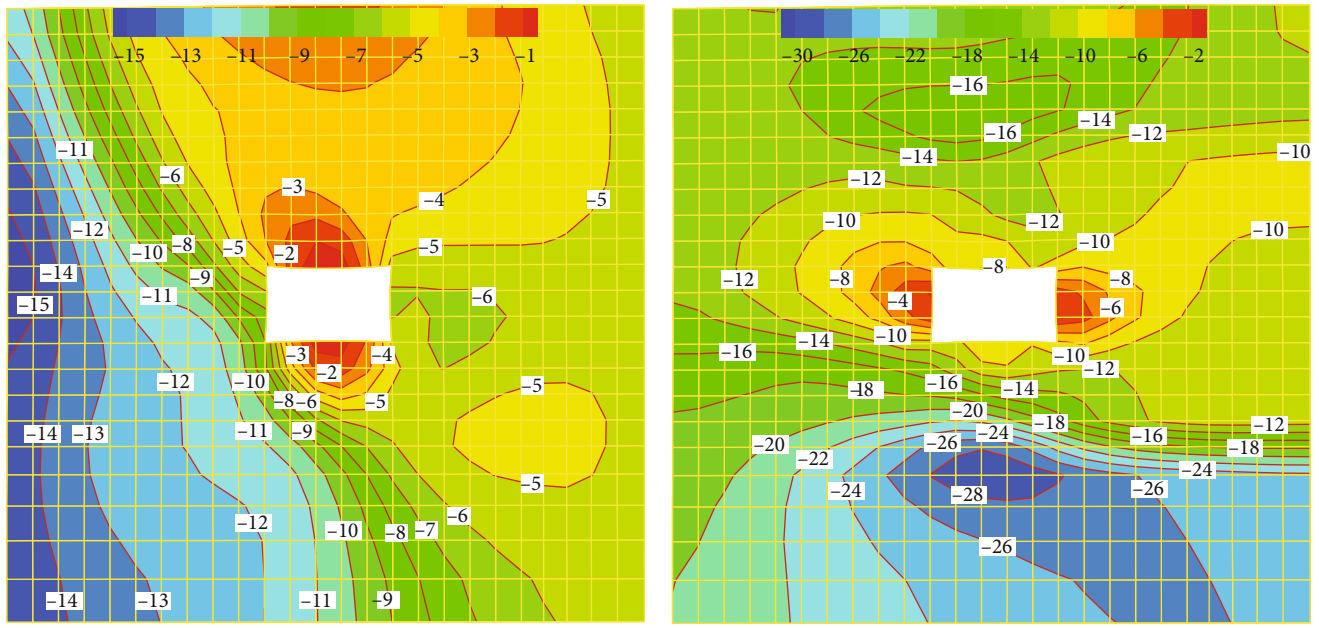

(a) Vertical stress (b) Horizontal stress

Figure 19: Distribution law of stress field in surrounding rock of roadway after mining.

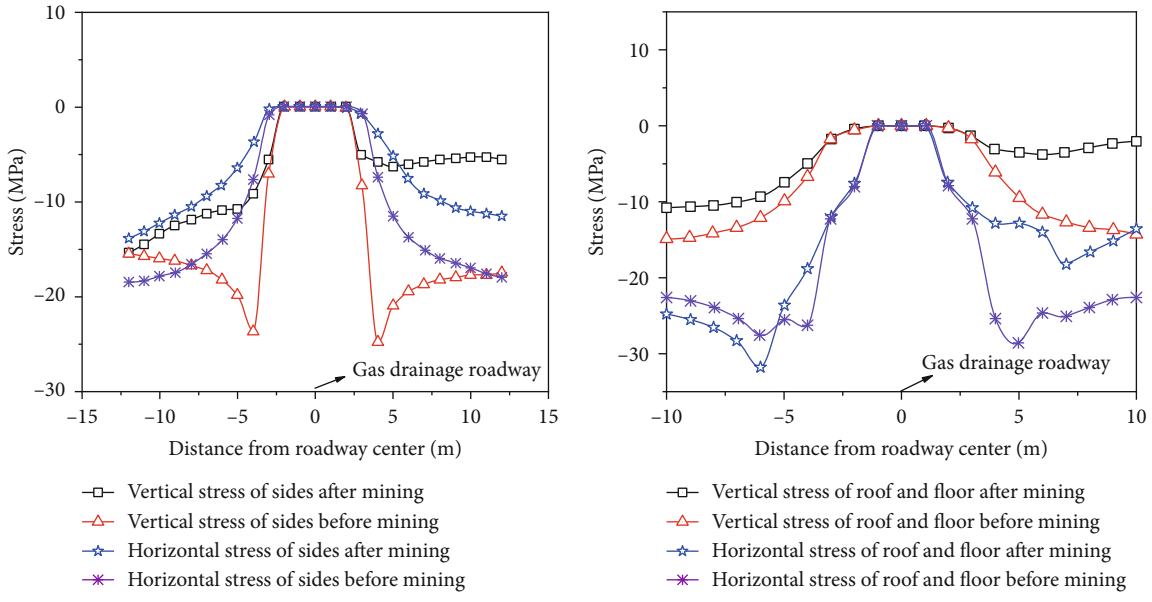

(a) Sides (b) Roof and floor

Figure 20: Stress distribution curve of roadway surrounding rock after mining.

4.2.2. 12050 Working Face Transport Roadway Excavation. After the excavation of transport roadway in 12050 working face, the stress field distribution law of roadway surrounding rock is shown in Figures 17 and 18. Compared with the external staggered layout, the stress distribution of FGDR has no significant difference, but the stress distribution law of both sides of roadway presents basically opposite distribution law due to different pressure relief direction. In addition, after the excavation of the transport roadway, the roof subsidence is 61.0 mm, the floor heave is 56.3 mm, the left side is 42.4 mm, and the right side is 48.7 mm.

4.2.3. 12050 Working Face Mining. After mining in 12050 working face, the stress distribution law of surrounding rock of FGDR is shown in Figures 19 and 20.

(1) After 12050 working face mining, the vertical stress of two sides of FGDR changes greatly. The peak value

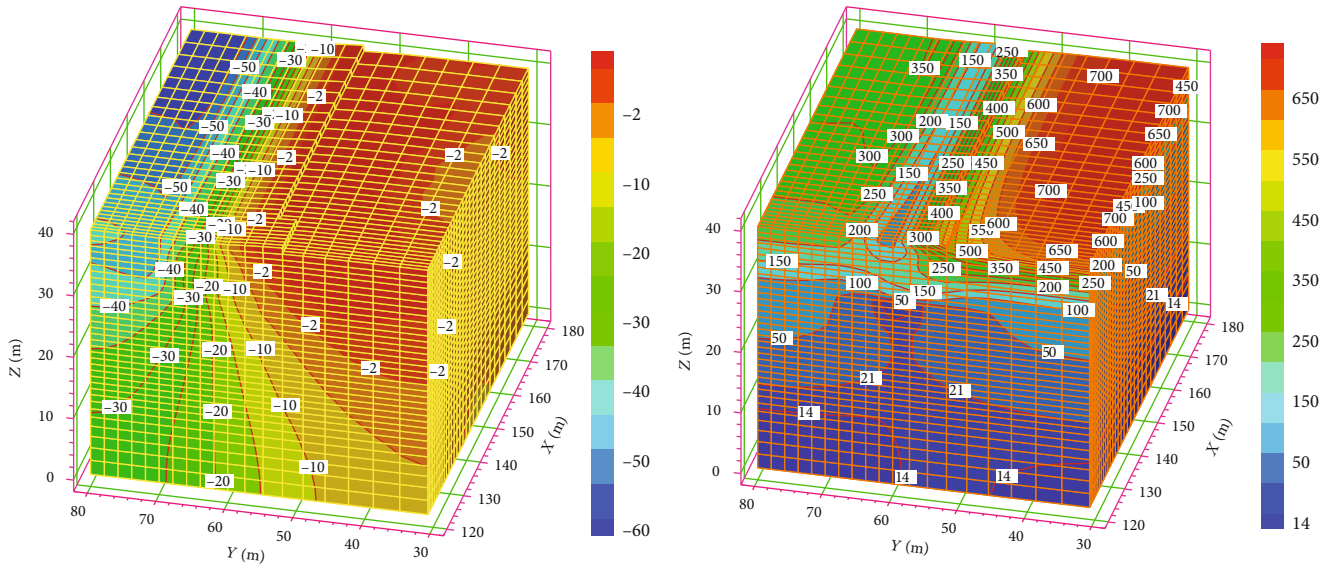

(a) Stress (b) Displacement

Figure 21: Distribution law of stress and displacement of surrounding rock after mining.

of vertical stress of left side is 2 m. The maximum stress difference is 14.6 MPa before and after mining. Compared with that before mining, the difference is 156.7%. When the depth is about 10 m, the vertical stress is basically the same before and after mining. The peak value of vertical stress on the right side is at depth 2 m. The maximum stress difference is 14.7 MPa before and after mining, which is 221.6% less than that before mining, and the depth is about 4 m. The vertical stress difference before and after mining is basically the same

(2) After 12050 working face mining, the horizontal stress of two sides of FGDR decreased greatly, and the change law of the two sides was basically the same: as far away from the roadway surface, the horizontal stress gradually increased, but the increase gradually decreased and finally tended to be stable; compared with before mining, the maximum reduction value of the left side horizontal stress was 6.2 MPa, which was at the depth of 6 m. The maximum reduction of horizontal stress on the right side is 6.4 MPa, and the depth is 10 m. With the distance from the end of the working face, the horizontal stress difference of the right side of the roadway increases gradually before and after mining

(3) After mining in 12050 working face, the vertical stress of FGDR roof and floor is reduced. With the distance away from the roadway surface, the stress difference before and after mining gradually increases, especially in the roof, the maximum reduction value is 12.9 MPa. After mining, the maximum vertical stress of roof is only 3.84 MPa, and the maximum vertical stress is 5 m deep

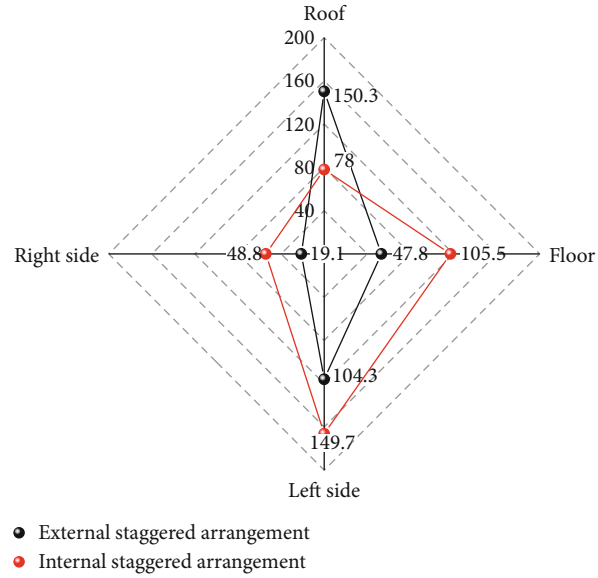

Figure 22: Deformation of surrounding rock of roadway with different layouts.

(4) After mining in 12050 working face, the horizontal stress at the roof of FGDR changes greatly, and the horizontal stress of floor increases. Within the depth of 5-6 m, the horizontal stress of the same position before and after mining is equal; the horizontal stress difference of roof before and after mining changes greatly, the maximum value is 4 m deep, the maximum decrease value is 15.5 MPa, and the decrease rate is 119.2%

To sum up, the mining face has a great influence on the vertical stress and horizontal stress of the surrounding rock

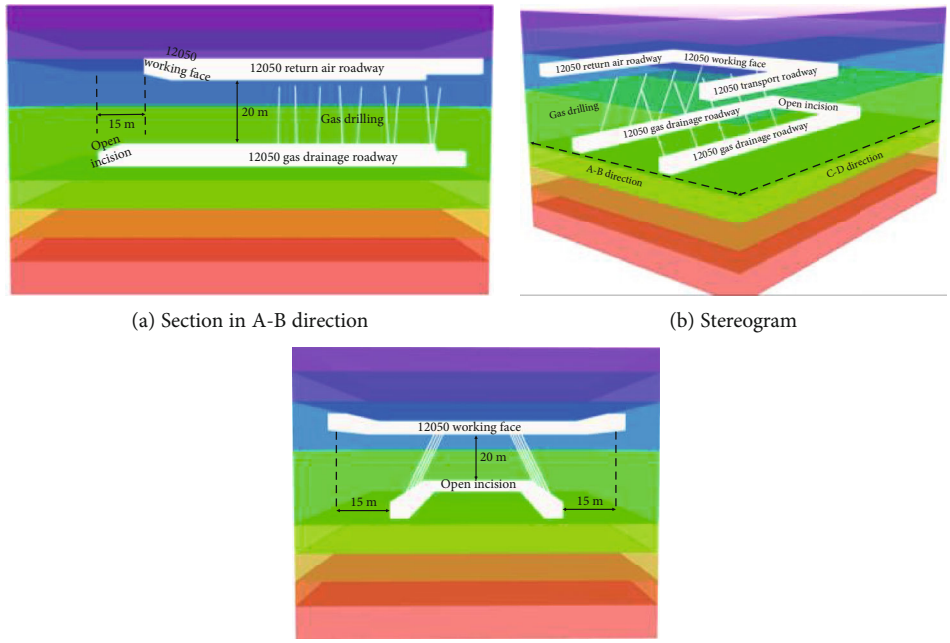

(a) Section in A-B direction

(b) Stereogram

(c) Section in C-D direction

Figure 23: Layout of FGDR and its open-off cut.

of the FGDR, and the vertical stress of the right side is the biggest. In addition, after mining, the roof subsidence of FGDR is 78.0 mm, the floor heave is 105.5 mm, the left side is 149.7 mm, and the right side is 48.8 mm.

4.3. Determination of the Position of Open-Off Cut in FGDR. The vertical distance between the open-off cut of FGDR and No. 15 coal seam is 20 m. After 12050 working face is mined, the distribution law of surrounding rock stress and displacement is shown in Figure 21.

(1) The outer side of 12050 working face is the stress increasing area, the area with horizontal distance more than 15 m from the working face changes gently, the displacement range is between 50 and 100 mm, and the stress concentration coefficient is about 1.4, which is a more reasonable open-off cut layout area of FGDR

(2) Under the goaf of the working face is the stress reducing area, but the advanced support stress is large during the roadway driving, and the surrounding rock deformation is serious. When the vertical distance is 20 m from the No. 15 coal seam, the surrounding rock deformation is large, and the service time of the FGDR open-off cut is longer, so it is not suitable to be arranged under the goaf

To sum up, the open-off cut of the FGDR should be arranged outside the working face and the horizontal distance from the working face is greater than 15 m. Considering the need of gas drainage, the vertical distance between the FGDR and the working face is 20 m, and the horizontal distance is 15 m.

4.4. Determination of Position of FGDR. After the 12050 working face is mined, the deformation of the surrounding rock of the roadway is shown in Figure 22 when the external and internal staggered layouts are carried out. The displacement of the roof and floor and the displacement of two sides are 198.1 mm and 183.5 mm and 123.4 mm and 198.5 mm, respectively, when the external and internal staggered layouts are carried out. Compared with the external staggered layout, the two sides of the roadway move closer, but the roof subsidence is significantly reduced, the safety factor of the roadway is significantly improved, and the vertical stress peak value of the left side of the roadway is more than 40 MPa; the surrounding rock is in a high stress environment for a long time, which is not conducive to the stability of the whole roadway, significantly reducing the gas drainage effect and increasing the safety risks of the working face. Although the floor heave of the roadway is large, the surrounding rock of the working face is in a low stress environment for a long time after mining, which is conducive to the long-term stability of the roadway. Therefore, the layout of FGDR is determined as internal staggered layout.

To sum up, internal staggered layout is the FGDR, with a vertical distance of 20 m from 12050 working face and 15 m horizontal distance from the end of 12050 working face; external staggered layout is adopted by the open-off cut of FGDR, with a vertical distance of 20 m from 12050 working face and 15 m horizontal distance with the open-off cut of 12050 working face. The specific spatial position relationship is shown in Figure 23.

5. Conclusions

(1) Based on the limit equilibrium theory, the stress distribution in the lateral plastic zone and elastic zone of

the working face is derived. Based on the semi-infinite plane mechanical model, the vertical stress and horizontal stress distribution of the floor is derived. The results show that the stress distribution in the range of 20 m from the back of the working face to 20 m in the front and 30 m below the floor is deduced

(2) Through numerical simulation and analysis, the distribution and evolution characteristics of surrounding rock stress and displacement field under the superposition of self-weight stress, excavation disturbance stress, and mining support stress are obtained. Based on this, the reasonable layout positions of FGDR under internal and external staggered layouts are determined: the layer with more than 20 m below the working face floor, the region with 10-15 m in front of the working face and 10-15 m behind the working face

(3) Considering the length of the gas drainage hole and the evolution characteristics of the floor stress distribution, two reasonable positions of the FGDR are preliminarily selected. Through numerical simulation, the stress and displacement distribution law of the surrounding rock of the FGDR at different positions are studied, and the reasonable layout mode of the FGDR is determined: internal staggered layout is the FGDR, with a vertical distance of 20 m from 12050 working face and 15 m horizontal distance from the end of 12050 working face; external staggered layout is adopted by the open-off cut of FGDR, with a vertical distance of 20 m from 12050 working face and 15 m horizontal distance with the open-off cut of 12050 working face

Data Availability

The data used to support the findings of this study are available from the corresponding authors upon request.

Conflicts of Interest

The authors declare that they have no conflicts of interest.

Acknowledgments

This work was supported by the National Natural Science Foundation of China (grant numbers 51904296, 52074240, and 51974296), the Outstanding Backbone Teachers of "Innovation Project" of University in Jiangsu Province, China, in 2020, and Major Projects of Natural Science Foundation of Universities in Jiangsu Province, China (grant number 20KJA560001). The sources of this support are gratefully acknowledged.

References

[1] B. Belle and M. Biffi, "Cooling pathways for deep Australian longwall coal mines of the future," *International Journal of Mining Science and Technology*, vol. 28, no. 6, pp. 865–875, 2018.

[2] S. Shreedharan and P. Kulatilake, "Discontinuum-equivalent continuum analysis of the stability of tunnels in a deep coal mine using the distinct element method," *Rock Mechanics and Rock Engineering*, vol. 49, no. 5, pp. 1903–1922, 2016.

[3] Q. Wojtecki, P. Konicek, and J. Schreiber, "Effects of torpedo blasting on rockburst prevention during deep coal seam mining in the Upper Silesian Coal Basin," *Journal of Rock Mechanics and Geotechnical Engineering*, vol. 9, no. 4, pp. 694–701, 2017.

[4] A. A. Sewell, "In deep: the boom and bust of the coal mining industry through the eyes of Black Appalachians," *Ethnic and Racial Studies*, vol. 42, no. 13, pp. 2333–2338, 2019.

[5] H. P. Xie, Y. Ju, S. H. Ren, F. Gao, J. Z. Liu, and Y. Zhu, "Theoretical and technological exploration of deep in situ fluidized coal mining," *Frontiers in Energy*, vol. 13, no. 4, pp. 603–611, 2019.

[6] D. K. Liu, Z. L. Gu, R. X. Liang et al., "Impacts of pore-throat system on fractal characterization of tight sandstones," *Geofluids*, vol. 2020, Article ID 4941501, 17 pages, 2020.

[7] H. Jing, J. Wu, Q. Yin, and K. Wang, "Deformation and failure characteristics of anchorage structure of surrounding rock in deep roadway," *International Journal of Mining Science and Technology*, vol. 30, no. 5, pp. 593–604, 2020.

[8] G. C. Li, Y. T. Sun, J. F. Zhang et al., "Experiment and application of coalcrete on roadway stability: a comparative analysis," *Advances in Materials Science and Engineering*, vol. 2020, Article ID 6813095, 14 pages, 2020.

[9] C. J. HOU, "Key technologies for surrouding rock control in deep roadway," *Journal of China University of Mining & Technology*, vol. 46, no. 5, pp. 970–978, 2017.

[10] X. M. Sun, F. Chen, C. Y. Miao et al., "Physical modeling of deformation failure mechanism of surrounding rocks for the deep-buried tunnel in soft rock strata during the excavation," *Tunnelling and Underground Space Technology*, vol. 74, pp. 247–261, 2018.

[11] H. P. Kang, P. F. Jiang, B. X. Huang et al., "Roadway strata control technology by means of bolting-modificationdestressing in synergy in 1 000 m deep coal mines," *Journal of China Coal Society*, vol. 45, no. 3, pp. 845–864, 2020.

[12] H. Y. Pan, D. W. Yin, N. Jiang, and Z. G. Xia, "Crack initiation behaviors of granite specimens containing crossing-double-flaws with different lengths under uniaxial loading," *Advances in Civil Engineering*, vol. 2020, Article ID 8871335, 13 pages, 2020.

[13] Y. Yu, D. Chen, X. Zhao, X. Wang, L. Zhang, and S. Zhu, "Stabilization mechanism and safety control strategy of the deep roadway with complex stress," *Advances in Civil Engineering*, vol. 2020, Article ID 8829651, 18 pages, 2020.

[14] X. F. Wang, C. G. Liu, S. J. Chen, L. Chen, K. Li, and N. Liu, "Impact of coal sector's de-capacity policy on coal price," *Applied Energy*, vol. 265, p. 114802, 2020.

[15] L. Xinjie, L. Xiaomeng, and P. Weidong, "Analysis on the floor stress distribution and roadway position in the close distance coal seams," *Arabian Journal of Geosciences*, vol. 9, no. 2, article 83, 2016.

[16] P. Wang, L. S. Jiang, C. Q. Ma, and A. Y. Yuan, "Evolution laws of mining-induced stress in floor strata and its influence on the stability of a floor roadway affected by overhead mining," *Earth Sciences Research Journal*, vol. 24, no. 1, pp. 45–54, 2020.

[17] S.-g. Li, H.-q. Shuang, H.-s. Wang, K.-I. Song, and L. Liu, "Extraction of pressurized gas in low air-conductivity coal seam using drainage roadway," *Sustainability*, vol. 9, no. 2, p. 223, 2017.

[18] Y. L. Xu, K. R. Pan, and H. Zhang, "Investigation of key techniques on floor roadway support under the impacts of superimposed mining: theoretical analysis and field study," *Environmental Earth Sciences*, vol. 78, no. 15, 2019.

[19] S. Mo, P. Sheffield, P. Corbett et al., "A numerical investigation into floor buckling mechanisms in underground coal mine roadways," *Tunnelling and Underground Space Technology*, vol. 103, article 103497, 2020.

[20] C. Zhu, M. C. He, M. Karakus, X. B. Cui, and Z. G. Tao, "Investigating toppling failure mechanism of anti-dip layered slope due to excavation by physical modelling," *Rock Mechanics and Rock Engineering*, vol. 53, no. 11, pp. 5029–5050, 2020.

[21] I. F. Oge, "Prediction of top coal cavability character of a deep coal mine by empirical and numerical methods," *Journal of Mining Science*, vol. 54, no. 5, pp. 793–803, 2018.

[22] X. Lai, H. Xu, P. Shan, Y. Kang, Z. Wang, and X. Wu, "Research on mechanism and control of floor heave of mining-influenced roadway in top coal caving working face," *Energies*, vol. 13, no. 2, p. 381, 2020.

[23] Y. Chen, S. Q. Ma, and Y. Yu, "Stability control of underground roadways subjected to stresses caused by extraction of a 10-m-thick coal seam: a case study," *Rock Mechanics and Rock Engineering*, vol. 50, no. 9, pp. 2511–2520, 2017.

[24] A. Vervoort and P. Y. Declercq, "Upward surface movement above deep coal mines after closure and flooding of underground workings," *International Journal of Mining Science and Technology*, vol. 28, no. 1, pp. 53–59, 2018.

[25] C. Zhu, X. D. Xu, W. R. Liu et al., "Softening damage analysis of gypsum rock with water immersion time based on laboratory experiment," *IEEE Access*, vol. 7, pp. 125575–125585, 2019.

[26] W. L. Shen, J. B. Bai, X. Y. Wang, and Y. Yu, "Response and control technology for entry loaded by mining abutment stress of a thick hard roof," *International Journal of Rock Mechanics and Mining Sciences*, vol. 90, pp. 26–34, 2016.